Materials Science & Engineering A 814 (2021) 141238

Contents lists available at ScienceDirect

Materials Science & Engineering A

journal homepage: http://www.elsevier.com/locate/msea

Microstructures and mechanical properties of Nb nanoparticles modified Ni60 hard-facing alloy fabricated by laser metal deposition

Liang Liu [a], Wenquan Wang [a], Xinge Zhang [a,*], Xin Li [a], Yingtao Tian [b], Xiaohui Zhao [a]

[a] College of Materials Science and Engineering, Jilin University, Changchun, 130025, PR China
[b] Department of Engineering, Lancaster University, Bailrigg, Lancaster, LA1 4YW, United Kingdom

ARTICLE INFO

Keywords:
Laser metal deposition
Ni60
Ni–Cr–B–Si alloy
Cracking problem
Nanoparticle

ABSTRACT

Crack-free samples were made from Nb nanoparticles modified Ni60 hard-facing alloy using laser metal deposition. Addition of Nb nanoparticles was carried out to modify the columnar dendrites and eutectic microstructures by providing large number of nucleation sites. The purpose of this study was to evaluate the effect of nanoparticles addition on cracking susceptibility of Ni–Cr–B–Si alloy. The results show that with addition of Nb nanoparticles, the cracking susceptibility reduced significantly with acceptable hardness loss. Large hard phases were refined and the columnar dendrites were converted to equiaxed grains, leading to a separated eutectic microstructure which restrain the initiation and growth of cracks. The study demonstrated a new method to tackle the cracking problem of laser manufactured Ni–Cr–B–Si alloys, accelerating the adoption of Ni–Cr–B–Si alloys on additive manufacturing applications.

1. Introduction

Ni60 alloy is one of Ni–Cr–B–Si system hard-facing alloys with high hardness, good wear resistance and self-fluxing property [1]. It is widely used in applications requiring high hardness and wear resistance [2]. In recent years, researches on the alloys are mainly concentrated on laser cladding [2–9], while there are few reports about 3D printing [10–14]. With the development of additive manufacturing technology, Ni–Cr–B–Si alloy has a good potential in the field of repairing and free-form manufacturing [15,16]. Laser metal deposition (LMD) which is also called 3D printing, is a technology that can build up metal components layer by layer from computer aided design (CAD) files. The technology increases the freedom of design and shortens the lead-time.

However, high-alloy grade Ni–Cr–B–Si alloy has high cracking susceptibility during laser manufacturing [7]. This seriously limits the application of the Ni–Cr–B–Si alloys in LMD. In order to solve the cracking problem, many efforts have been made, including preheating [17], slow cooling and addition of toughing agents [18,19]. During the laser manufacturing process, the high cooling rate can lead to great stress. The methods of preheating and slow cooling can reduce the generation of stress, but the cost is high, and it is not applicable in some practical situations. As a result, adding toughing composition to modify the microstructure of Ni–Cr–B–Si alloy is a better choice to solve the cracking problem.

The phase constitution of laser manufactured Ni–Cr–B–Si alloy is mainly composed of the hard phases of Cr borides and carbides, dendrites of Ni and eutectics of Ni–B–Si [20]. At present, many studies focus on refining large hard phases in the alloy [21]. Large Cr precipitates are hard and brittle, so it is easy for cracks to initiate and grow through Cr precipitates. The observation of microstructure showed that cracks can grow through the Cr hard phases. The maximum stress (σ_m) of a fractured hard phase grain can be described by the formulation as:

$$\sigma_m = 2\sigma_a\sqrt{\alpha/\rho_c}$$

Where σ_a is the applied stress, ρ_c is the radius of curvature of the crack and α is the length of the crack (the size of the grain) [22]. Therefore, the refinement of large Cr hard phases, i.e. smaller α, is expected to decrease cracking susceptibility of the alloy.

Elements that have been used to refine the microstructure of the alloy include Ti, V, Ta, Zr and Nb [18,19,21,23,24]. The mechanism of the refinement is to provide nucleation sites to Cr hard phases. However, the addition of Ti, V, Ta, Zr either fails to refine the microstructures or refine the microstructures while deteriorating the hardness. Among the attempts, the addition of Nb has the best result, which can refine the large Cr hard phases with acceptable hardness loss. Nb has a higher

* Corresponding author.
E-mail address: zhangxinge@jlu.edu.cn (X. Zhang).

https://doi.org/10.1016/j.msea.2021.141238
Received 15 December 2020; Received in revised form 17 March 2021; Accepted 3 April 2021
Available online 7 April 2021
0921-5093/

Table 1
Chemical compositions of Ni60 powders (wt.%).

Element	Ni	Cr	B	Si	Fe	C
wt.%	Bal.	16.00	3.20	4.00	<15.00	0.80

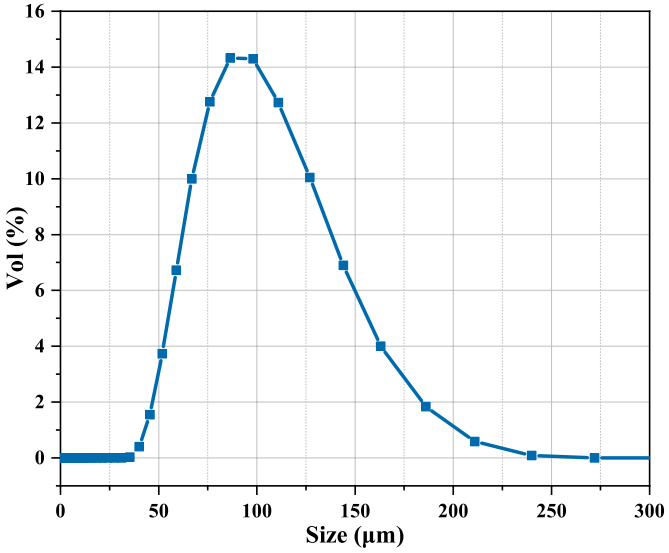

Fig. 1. Particle size distribution of Ni60 powder.

affinity for B and C than Cr has. What's more Nb precipitates have a higher formation temperature than that of Cr carbides and borides and a low solubility in Cr precipitates. So Nb precipitates can act as good nucleation sites in the alloy. However, the result shows that even though hard phases are refined while maintaining the hardness almost the same as original alloy, the cracking susceptibility doesn't decrease [18,19].

In our previous research, the Ni–Cr–B–Si alloy tends to form large amount of Ni columnar dendrites and Cr precipitate dendrites during LMD [14]. And there are continuous eutectic structures between the dendrites and Cr hard phases. The eutectic structures are hard and brittle phases which may also have a great influence on cracking susceptibility of Ni–Cr–B–Si alloy. As reported in previous studies, the addition of Nb can refine the Cr hard phases but there are still dendrites and continuous eutectics remained in the alloy which may provide paths for crack growth [18,19]. The modification of dendrites and eutectics may be a new method to solve the cracking problem of Ni–Cr–B–Si alloy. There has been report of improvement in crack tendency of Al alloy by modifying columnar dendrites [25]. Nanoparticles were added in Al alloy powders before manufacturing and crack-free samples were built

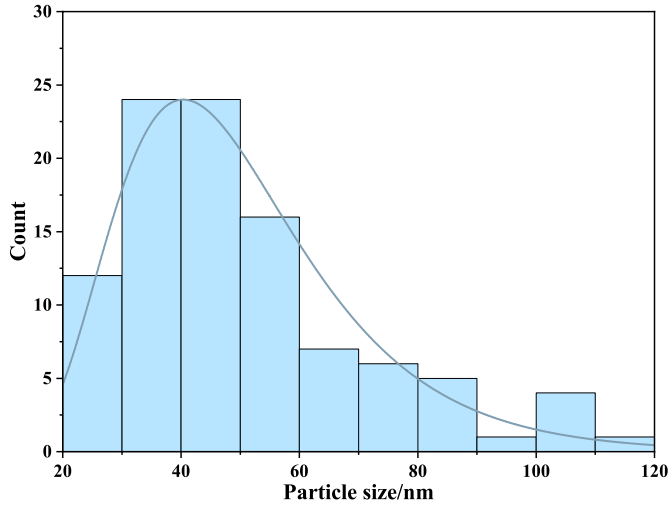

Fig. 3. Particle size distribution of Nb nanoparticles.

Table 2
Ball mailing parameters.

Rotation speed (rpm)	Ball-to-powder weight ratio (%)	Milling time (h)
250	0	3

by selective laser melting (SLM). Based on the report, it seems that the addition of nanoparticles can be a viable method to improve the cracking performance of Ni–Cr–B–Si alloy.

In this study, different amount of Nb nanoparticles were added to Ni–Cr–B–Si hard-facing alloy (Ni60) to refine the columnar dendrites and eutectics. The purpose of the research is to find the effect of Nb nanoparticles addition on cracking susceptibility and the mechanism of microstructure refinement and phase formation. The outcome of this study can enhance the understanding of cracking mechanism of Ni–Cr–B–Si alloy, and promote the adoption of the alloy on LMD applications.

2. Experimental procedure

2.1. Materials and LMD parameters

Ni60 alloy (particle size about 50–150 μm) was selected as the original alloy for further modification by Nb nanoparticles. The alloy was provided by Shanghai Global Fusion Materials Technology Co., Ltd, and chemical compositions of the alloy are presented in Table 1.

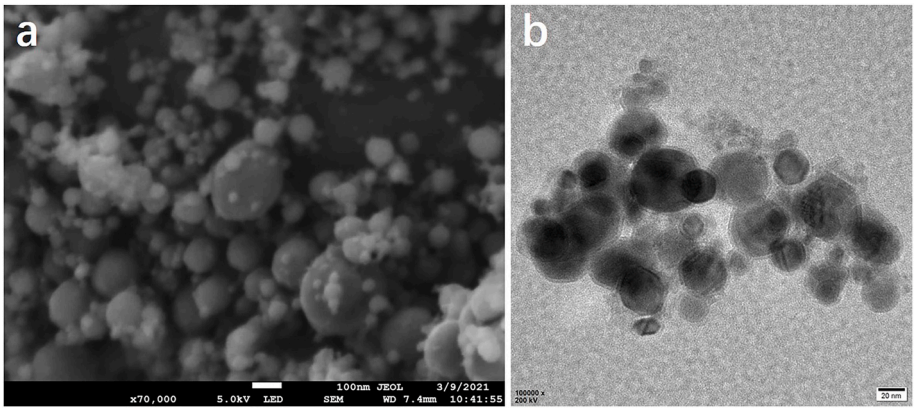

Fig. 2. (a)SEM image of Nb nanoparticles (b) TEM image of Nb nanoparticles.

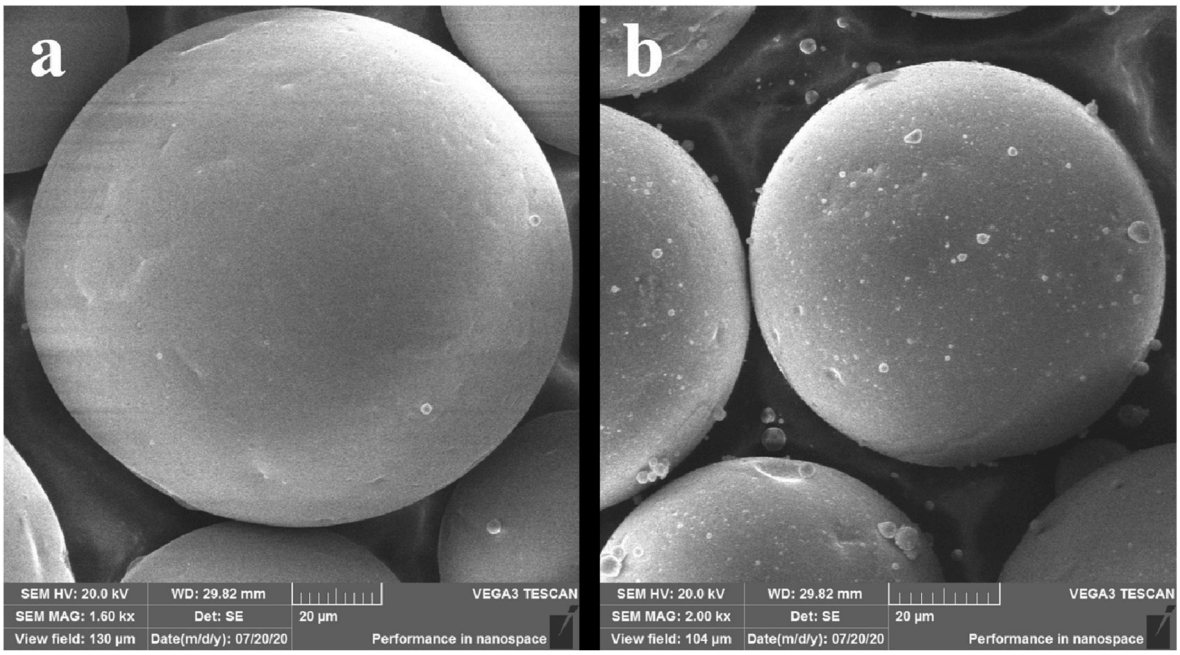

Fig. 4. Morphology of (a) Ni60 powders and (b) Nb nanoparticles modified Ni60 powders.

Table 3
Parameters of LMD.

Laser power/W	Scan speed/ $mm{\cdot}s^{-1}$	Spot diameter/mm	Powder feed rate/$g{\cdot}min^{-1}$	Z increment/ mm
400	2	1.25	7.3	0.9

The size distribution of Ni60 particles was measured using Mastersizer3000 particle size analyzer. Fig. 1 shows the distribution of particle size. Approximately 80% of particle volume locates in the size zone between 63.9 μm and 153 μm.

The Nb nanoparticles used in the experiment were provided by Shanghai Yao Tian Nano Material Co., Ltd with size about 50 nm. Due to the tiny scale of nanoparticles, the size analysis was conducted by counting from SEM pictures. Fig. 2 shows the SEM and TEM pictures of Nb nanoparticles. Fig. 3 shows the size distribution of Nb nanoparticles.

The average size of Nb nanoparticles is about 50.2 nm. Most of nanoparticles are smaller than 100 nm.

Nanocomposite feed stock was prepared right before the experiment by a planetary-type ball mill (XQM-4) in case of settling. Ball mailing parameters were shown in Table 2. Fig. 4 shows the morphology of Ni60 powders and Nb nanoparticles modified Ni60 powders.

The LMD platform used in the experiment consists of IRB1410-ABB robot (controlled by computer), gas protection system, powder feeder, coaxial powder injection nozzle and semiconductor laser unit (Raycus RFL-A1000D) . Argon was used as powder carrier and shielding gas. Thin wall samples of Ni60 and Nb nanoparticle modified Ni60 with the dimension of 20 mm (length) × 3 mm(width) × 35 mm(height) were built on the substrate of stainless steel with the dimension of 100 mm (length) × 50 mm(width) × 8 mm(height). Samples of different Nb nanoparticles addition were built including 0.5 wt%, 1 wt%, 1.5 wt%, 2 wt%, 2.5 wt%, 3 wt% , and 5 wt%. The maximum addition of Nb nanoparticles in this research is 5 wt%, because the addition of nanoparticles deteriorates the liquidity of feed stock. To ensure the good forming, process parameters were optimized by conducting numerous single-track tests in advance [26]. Table 3 shows the parameters of LMD used in the experiment.

2.2. Microstructural characterization

After deposition, samples were separated from the substrate by wire-electrode cutting. Samples for morphology observation and hardness test were cut from the transverse section and prepared by standard

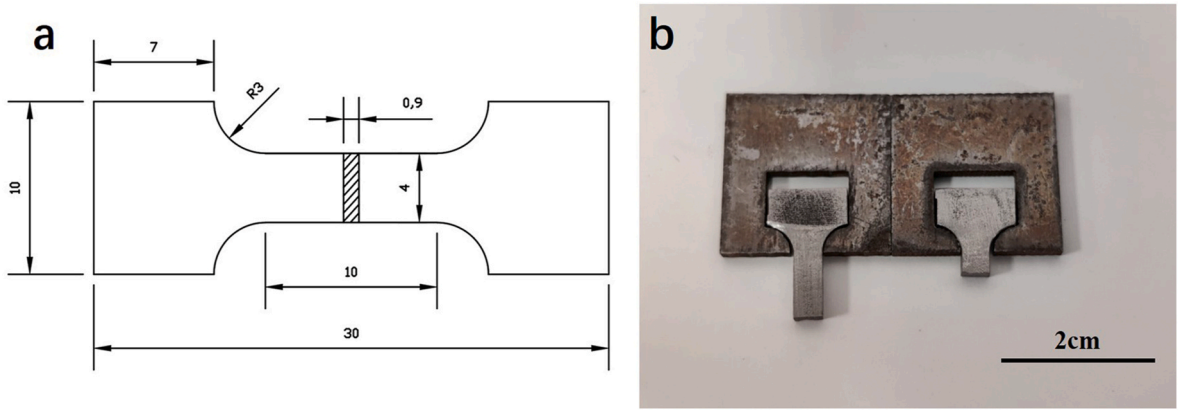

Fig. 5. (a) Tensile test specimen (mm) and the (b) fixtures.

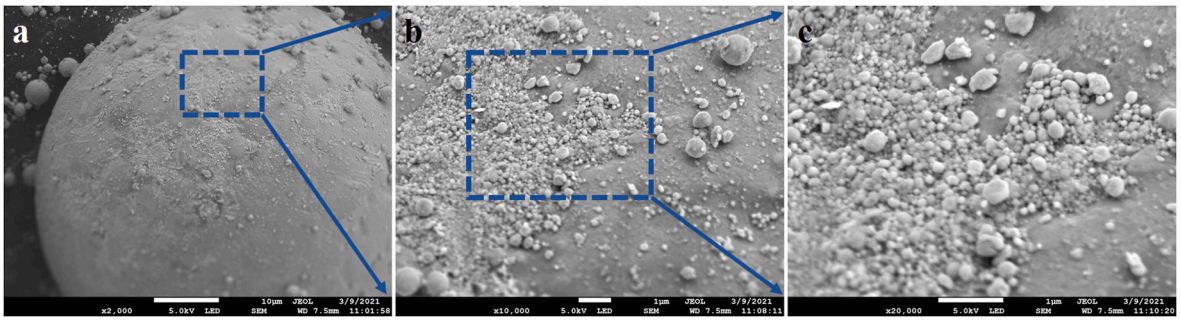

Fig. 6. Morphology of Nb nanoparticles attached to the surface of Ni60 particle.

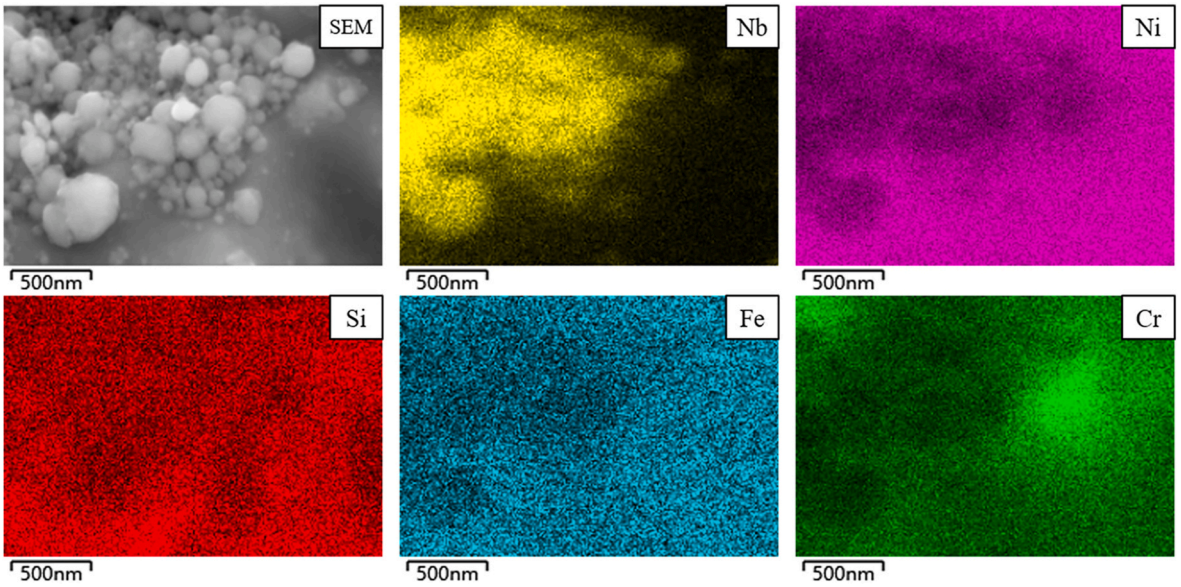

Fig. 7. EDS mapping of Nb nanoparticles on the surface of Ni60 powder.

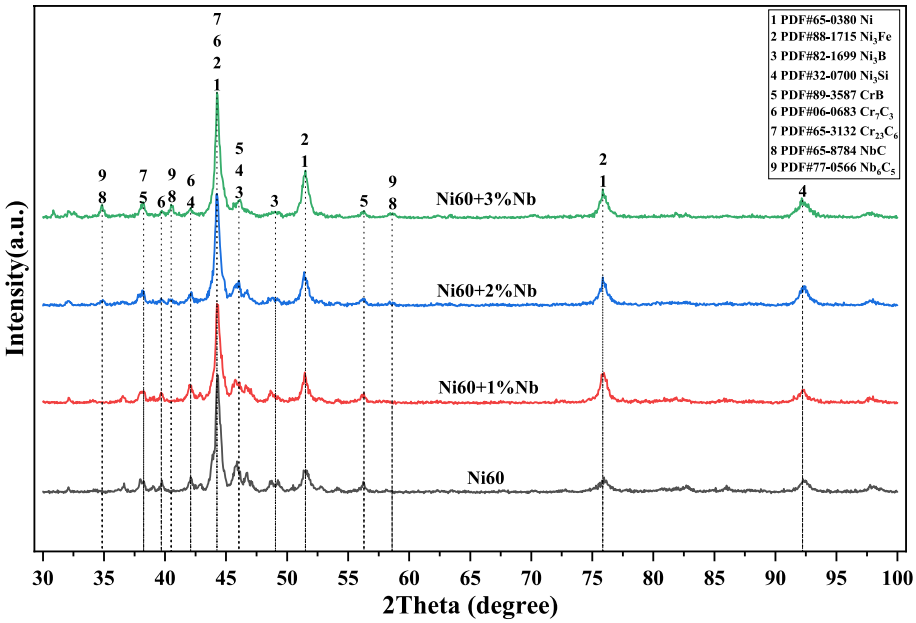

Fig. 8. XRD pattern of the sample modified by 0%, 1%, 2%, 3 wt% Nb.

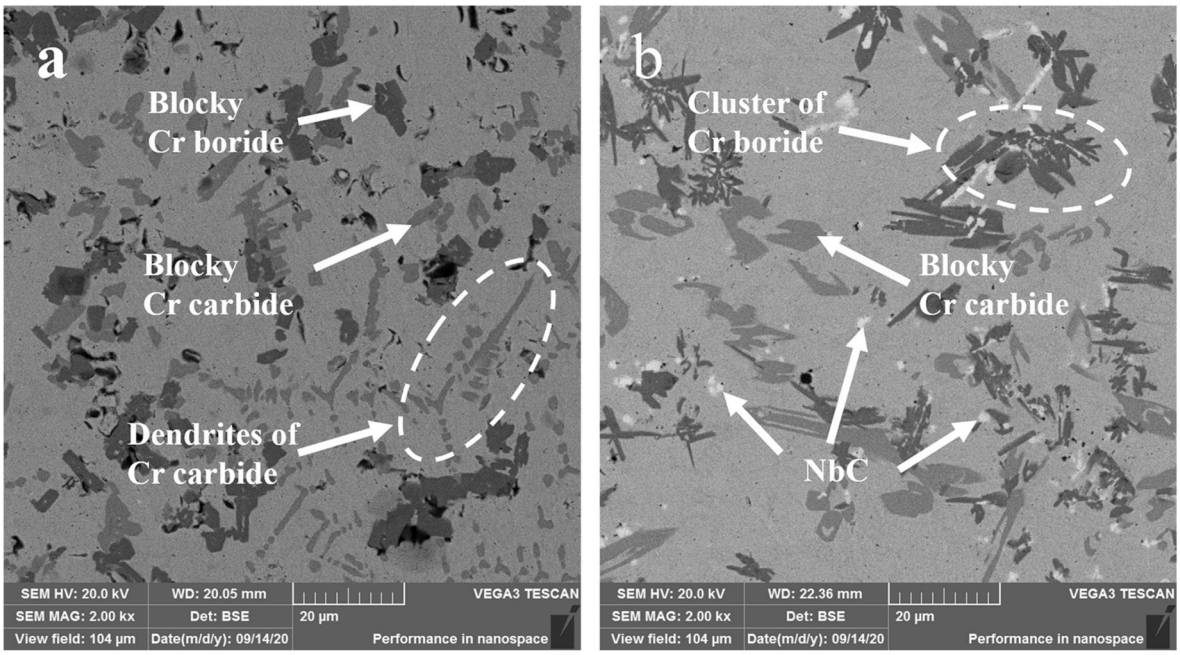

Fig. 9. As-polished SEM-BSE images with 0.5 wt% (a) and with 3 wt% (b) Nb.

mechanical grinding and polishing. Before optical microscopy (OM) and scanning electron microscopy (SEM) observation, some of the samples were etched by a solution of 20 ml HNO_3, 20 ml CH_3COOH and 30 ml HCl. OM (Zeiss Axio Imager A1m) , SEM (TESCAN VEGA3 and JSM-7900F) with energy dispersive spectroscopy(EDS) and XRD (X-ray diffraction/Rigaku D/Max 2500 PC, Cu Kα, 4°/min) were used for microstructure observation and phase identification.

2.3. Mechanical properties

Vickers hardness was measured on cross-section by MH-3 Vickers hardness tester at a loading force of 500 g and a loading time of 10s. Tensile tests were performed on MTS810 material testing system. Tensile specimens were cut by wire-electrode machining from LMD samples. Due to the brittleness of the specimen, fixtures were designed to prevent fracture at the fixing stage. Fig. 5 shows the tensile test specimen and the fixtures. During tensile tests, the upper part of the fixture was sent into the clamp to avoid crush of the sample.

3. Results

3.1. Powder characterization

After ball mailing, Nb nanoparticles were attached to the surface of Ni60 powder as show in Fig. 6. The surface of Ni60 powder were not completed covered by nanoparticles.

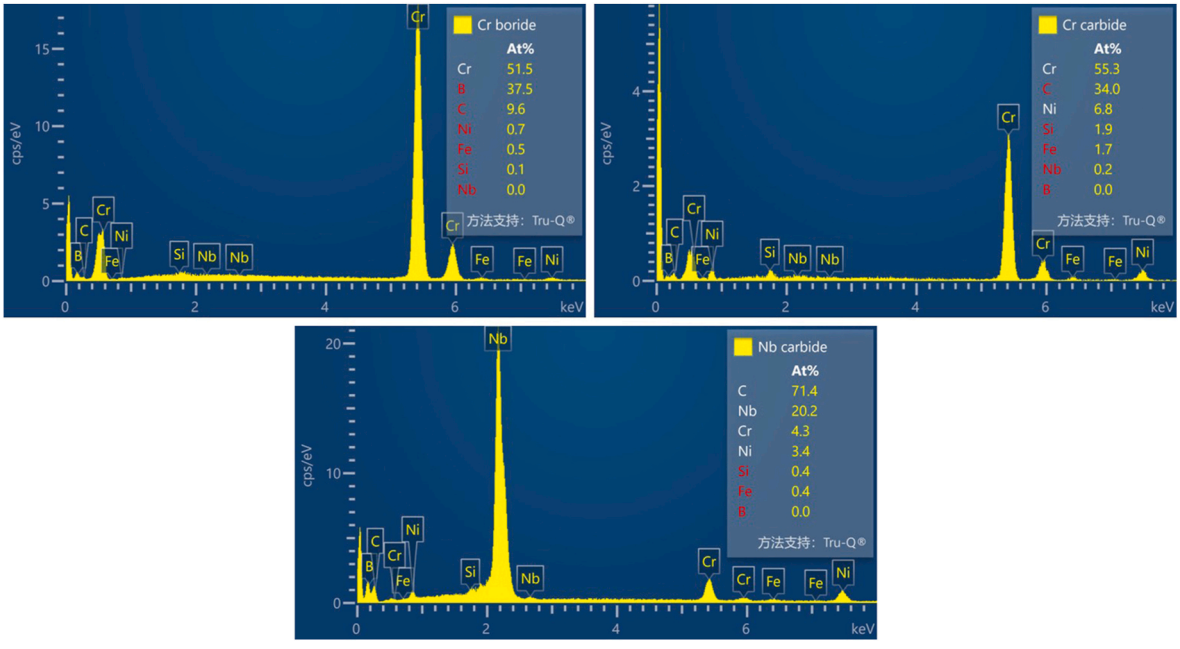

Fig. 10. EDS-point analysis of Cr boride, Cr carbide and Nb carbide in Fig. 9.

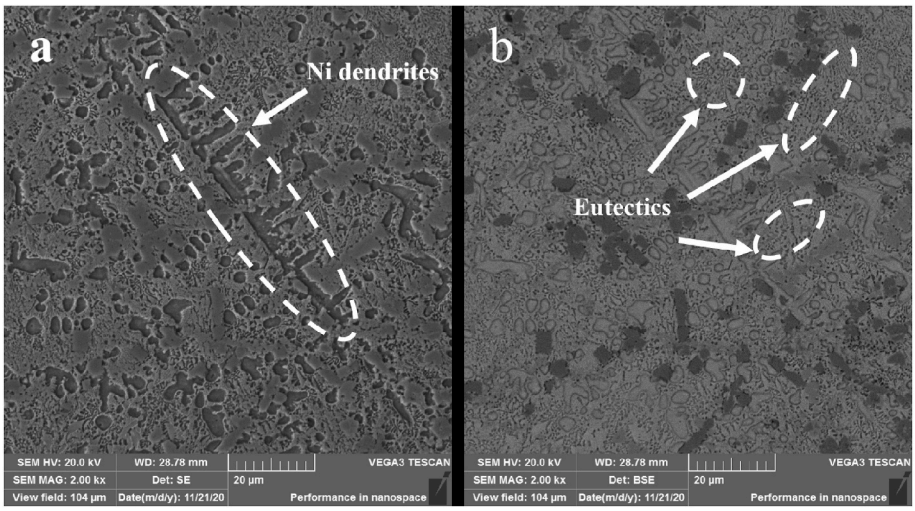

Fig. 11. (a) SE image of etched Ni60 sample. (b) BSE image in the same area.

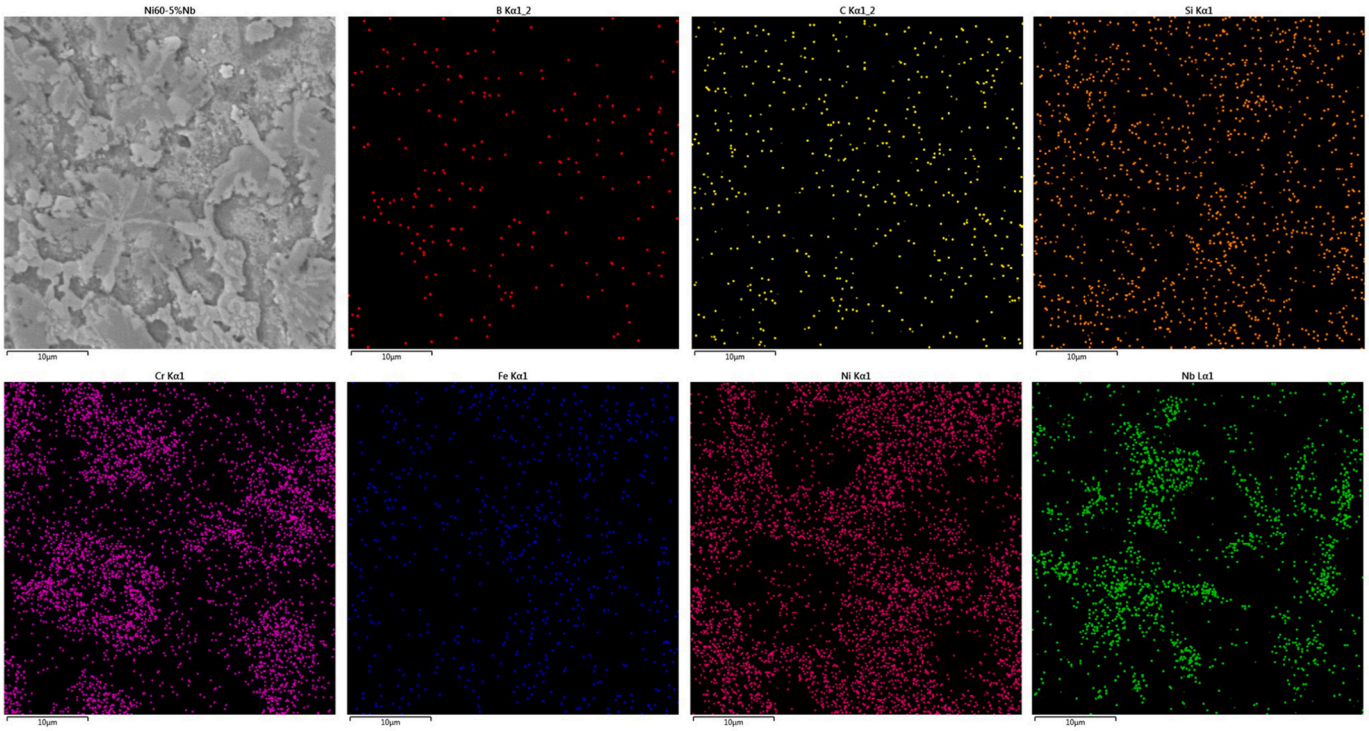

Fig. 12. EDS maps of the sample with 5 wt Nb%.

To ensure the presence of Nb nanoparticles, EDS mapping was carried out as shown in Fig. 7.

As shown in the EDS mapping, the nanoparticles that struck to the surface of Ni60 powder were Nb nanoparticles.

3.2. Phase identification of Nb nanoparticles modified sample

Because of the complexity of phase constitution, the phases were initially identified by XRD, and then verified by analysis of BSE and EDS. Fig. 8 shows XRD result of simple with 0%, 1%, 2%, 3 wt% of Nb.

According to the XRD data, the main phases in Nb nanoparticles modified sample include: Ni、Ni_3Fe、Ni_3B、Ni_3Si、CrB、Cr_7C_3、$Cr_{23}C_6$、NbC and Nb_6C_5. The diffraction peaks of NbC and Nb_6C_5 increase with the increase of Nb nanoparticles.

With XRD result, phases can be recognized by the brightness difference in SEM-BSE images. Because the intensity of back scattered electron beam is positively related with atomic number, so the phase with larger atomic number is brighter than the phase with smaller atomic number in BSE images. Fig. 9 shows the microstructures of as-polished simples using BSE.

Combined with the XRD analysis and EDS analysis in Fig. 10, it can be confirmed that the phases with light color in Fig. 9 are Cr carbides such as CrB and the dark hard phases are Cr borides such as Cr_7C_3 and $Cr_{23}C_6$. There are dendrites of Cr carbides, blocky Cr carbides and blocky Cr borides in the sample with 0.5% Nb. With the increase of Nb addition, dendrites of Cr carbides disappear and the morphology of Cr borides changes from blocky to cluster shape.

In Fig. 4(b), small white phases surrounded by Cr borides are Nb carbides. In accordance with equilibrium phase diagram of Nb–C, the Nb carbides are NbC (3600 °C) which forms at a much higher temperature

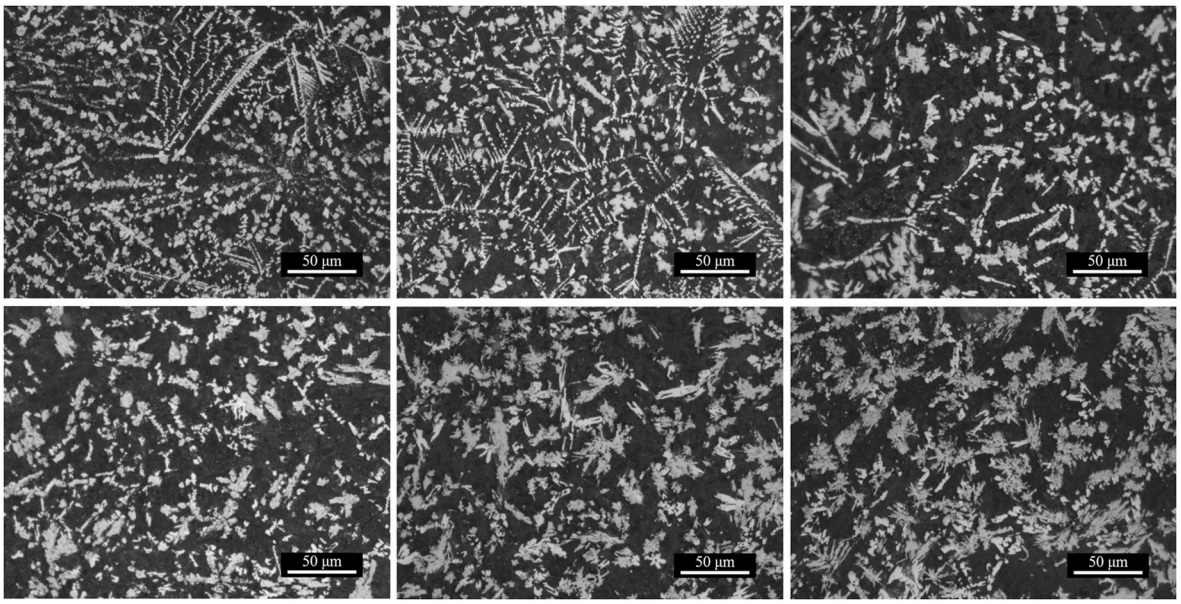

Fig. 13. OM images comparing the morphology of hard phases in samples with (a) 0 wt %, (b) 0.5 wt %, (c) 1 wt %, (d) 1.5 wt %, (e) 2 wt %, (f) 2.5 wt % Nb addition.

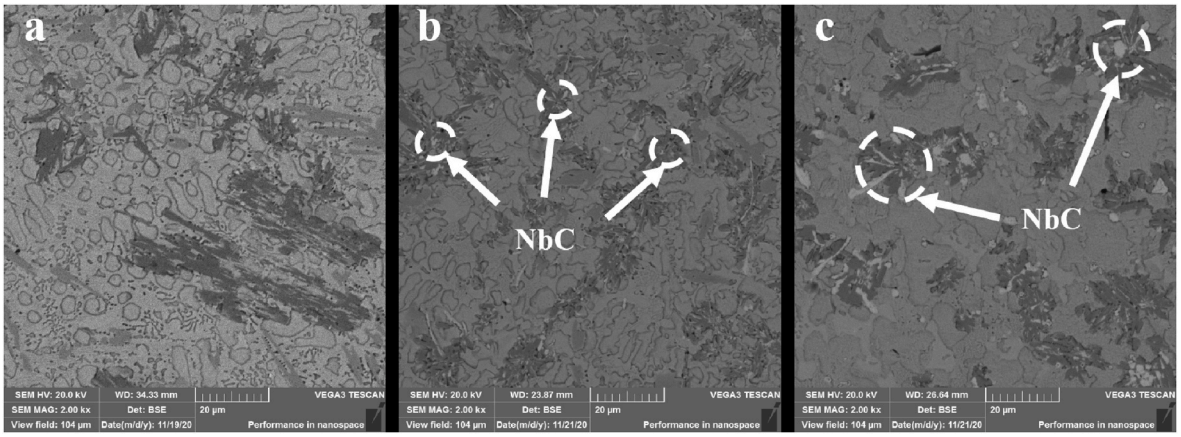

Fig. 14. SEM-BSE images of Ni60 with (a) 1.5 wt%, (b) 2 wt%, (c) 5 wt%.

than Nb_6C_5 (1050 °C).

The bright back ground consists of Ni dendrites and Ni–B–Si eutectics which have the same contrast in the BSE image of as-polished samples due to the large amount of Ni in the microstructures. However, they can be distinguished in the SEM image of etched sample as shown in Fig. 11.

Ni dendrites can be distinguished in Fig. 11 (a) because its

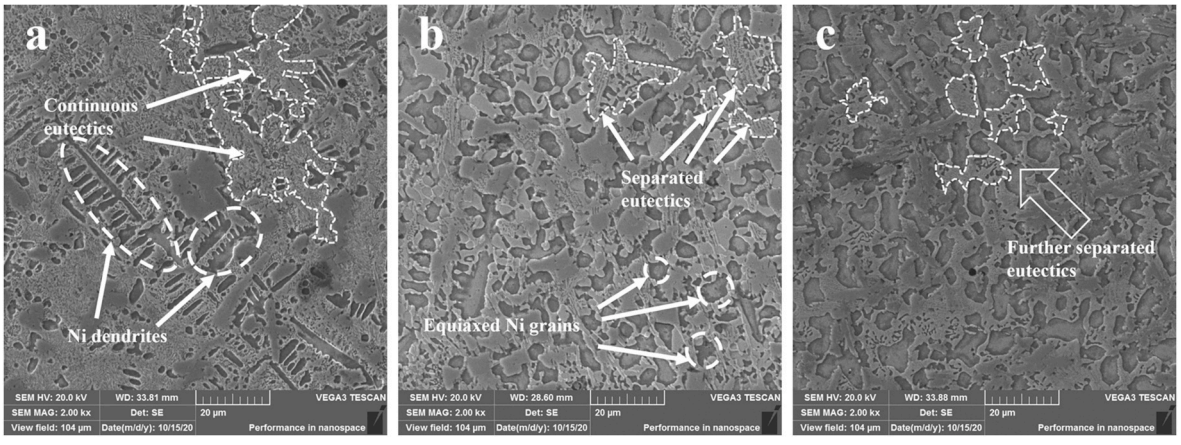

Fig. 15. SEM - SE image of (a) Ni60, (b) Ni60 with 0.5 wt % Nb, (c) 3 wt %.

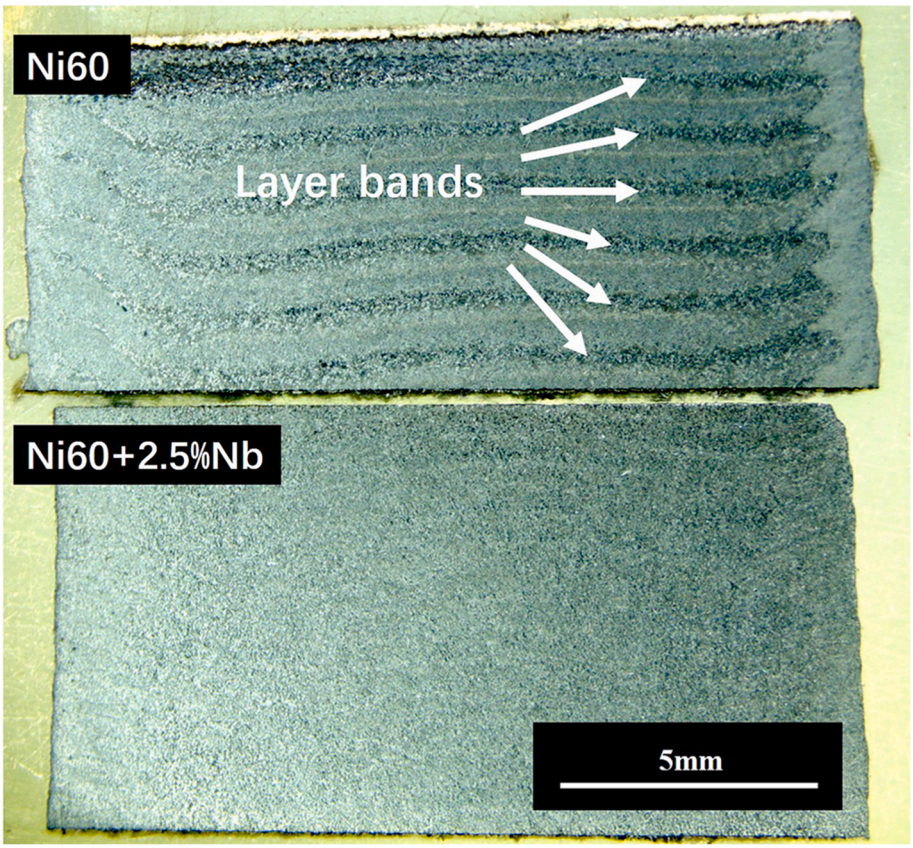

Fig. 16. Macro morphology of Ni60 and Ni60 with 2.5 wt % Nb.

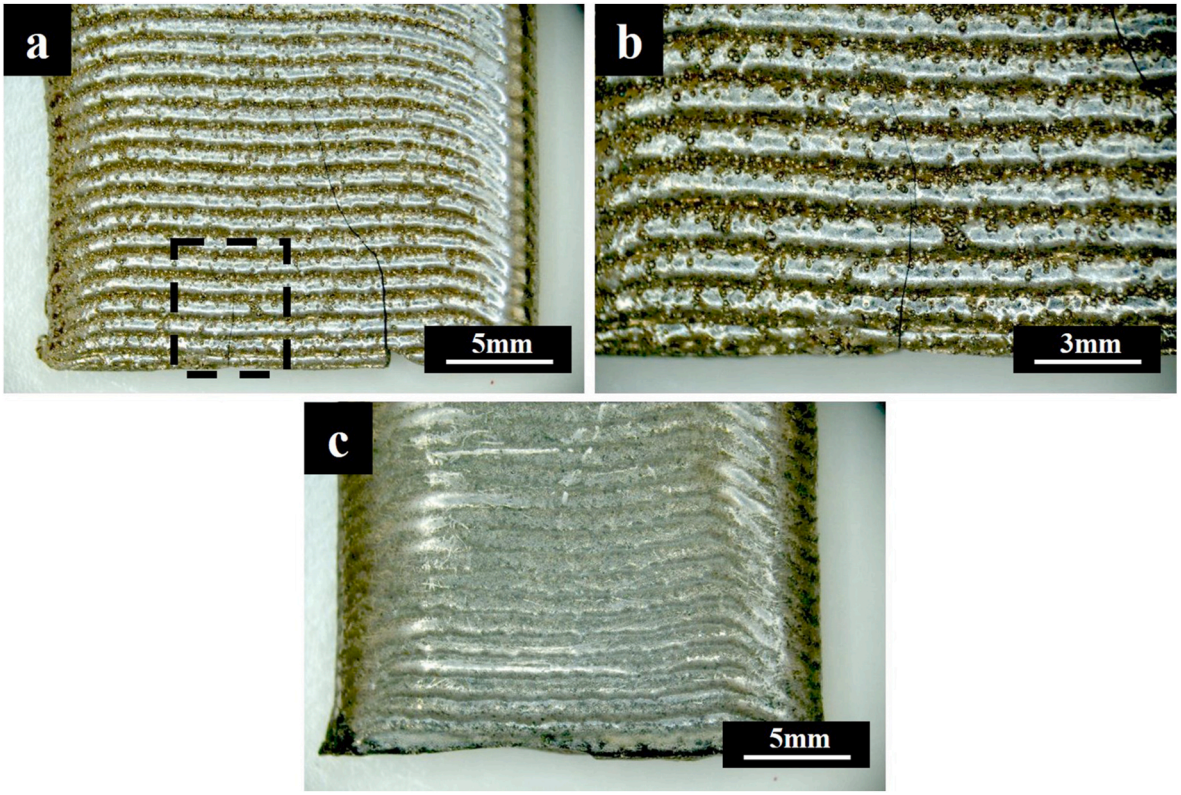

Fig. 17. Cracks in as-build sample of (a) Ni60, (b) enlarged view of framed area in (a), (c) Ni60 with 0.5 wt % Nb.

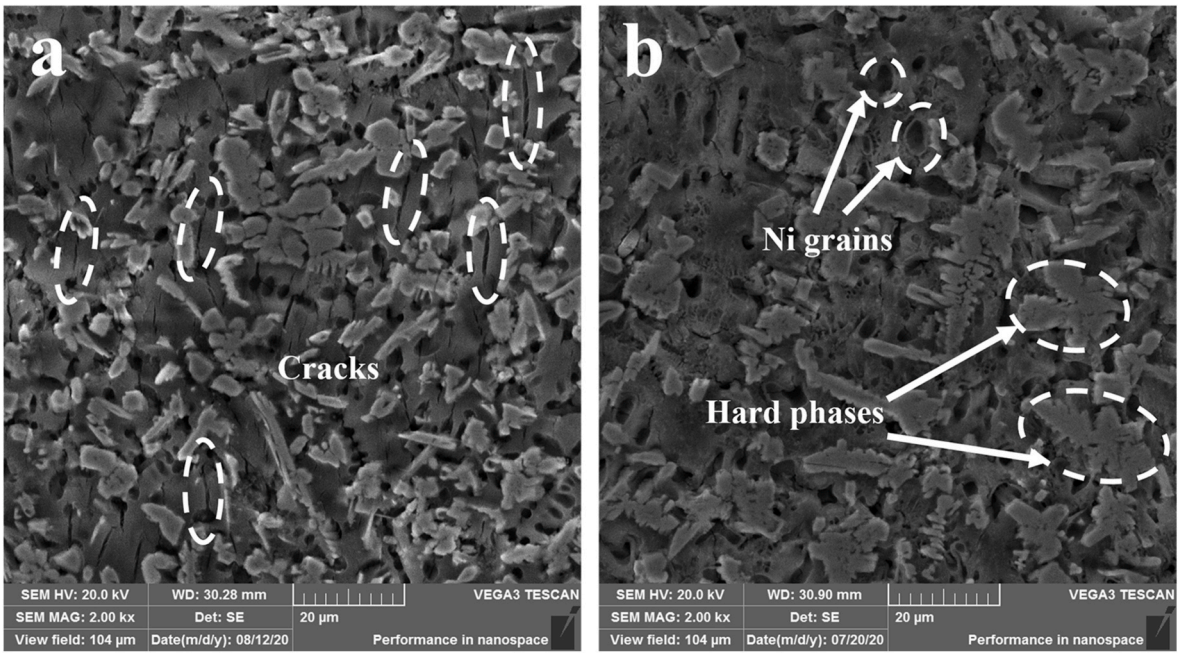

Fig. 18. SEM-BE of over-etched (a) Ni60 and (b) Ni60 with 1 wt% Nb.

susceptibility to the etching solution. Among the Ni dendrites and hard phases are layered eutectics containing Ni, Fe, B, Si, as shown in EDS maps (Fig. 12).

3.3. Microstructural changes with Nb nanoparticles addition

OM and SEM were used to investigate the changes of microstructures in Nb nanoparticles modified samples. Fig. 13 shows the morphology of Cr hard phases with Nb nanoparticles addition from 0 wt % to 2.5 wt %.

The Microstructure of hard phases changes significantly with the addition of Nb nanoparticles. With the increase of Nb nanoparticles addition, dendrites of Cr carbides decrease and finally disappear. The morphology of Cr borides changes from regular blocky shape to irregular cluster shape. The cause of the microstructures change is the in-situ formed NbC nucleation sites. Fig. 14 shows the SEM-BSE images of Ni60 with different Nb nanoparticles addition.

In the sample with Nb addition less than 2 wt%, NbC precipitates are invisible. In the samples with Nb addition above 2 wt%, they exist in the midst of Cr borides and grows with the increase of Nb. Besides the hard phases, Ni dendrites and Ni–B–Si eutectics are also influenced by the addition of Nb nanoparticles. Fig. 15 shows the microstructural changes of Ni dendrites and Ni–B–Si eutectics.

With the addition of Nb nanoparticles, Ni grains change from columnar dendrites to equiaxed grains. The continuous structure of Ni–B–Si eutectics is separated by equiaxed Ni grains and Cr hard phases. The modification effect of Nb nanoparticles on eutectics is obvious even in the sample with lowest Nb addition (in this case, 0.5 wt % Nb). In addition, eutectics can be further separated with the increase of Nb addition.

Fig. 16 shows the layer bands in Ni60 and Ni60 with 2.5 wt% Nb. The layer bands are clearly visible in the Ni60 sample as arrowed in the picture. Layer band is a structure that forms during the remelt of existing layer. As discussed in our former research, in LMD Ni60 sample, layer bands possess a lower hardness than the rest of the sample which deteriorate the homogeneity.

With the addition of Nb nanoparticles, layer bands became obscure and the homogeneity improved. Owing to the fast cooling rate and various cooling conditions, the microstructures of LMD Ni60 is heterogeneous. With the addition of Nb nanoparticles, the microstructures become more homogeneous. The size and number of columnar dendrites decrease gradually. The morphology of hard phases changes from regular shape to irregular.

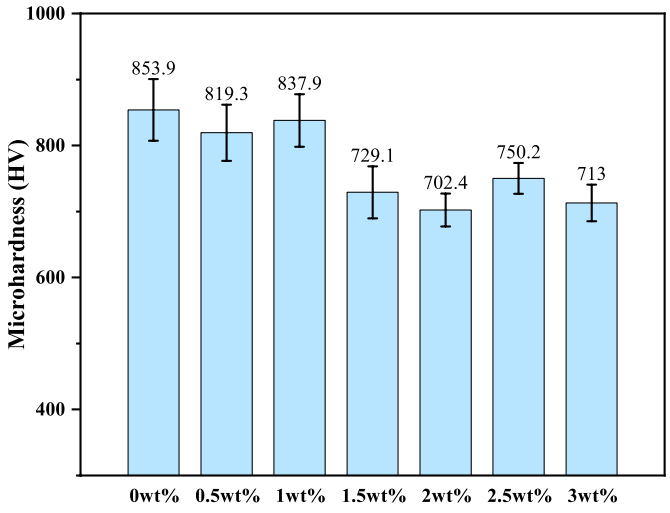

Fig. 19. Microhardness of Ni60 samples with different Nb nanoparticles addition.

What's more, it's worth noticing that the addition of excessive Nb nanoparticles (in this case, about 5 wt % Nb) is not good for powder feeding, which will weaken the powder fluidity and lead to uneven powder feeding quantity. In long-term building, this may cause blockage of powder feeding tube, resulting in poor building quality.

3.4. Cracking susceptibility and mechanical properties

Three samples were built for each Nb content, and all of the Ni60 samples have cracks and samples with addition of Nb nanoparticles are crack free. Fig. 17 shows as-build samples of Ni60 and Ni60 with 0.5 wt % Nb. Crack-free samples (Fig. 17 c) can be built with little amount of Nb nanoparticles addition. In Fig. 17 (a) and (b), 2 cracks can be observed and the longest one is about 10 mm. The cracks initiated from the

Table 4
Statistical analysis of microhardness.

Nb addition	0 wt %	0.5 wt %	1 wt %	1.5 wt %	2 wt %	2.5 wt %	3 wt %
Mean (HV)	853.9	819.3	837.9	729.1	702.4	750.2	713
Mean variance (HV)	46.6	42.8	39.9	39.4	24.9	23.3	27.7

junction between the substrate and sample, and grew up through layers.

Because the secondary electronic signal is sensitive to the morphological characteristics, so SEM - SE was used to identify cracks in samples. Fig. 18 shows the SEM - SE image of Ni60 and Ni60 with 1 wt % Nb. Both of the samples were over etched to observe the microcracks. In the over etched sample, Ni dendrites dissolved in the etching solution leaving etching pits as shown in Fig. 18. Ni–B–Si eutectics were etched heavily, so microcracks are clearly visible in Fig. 18 (a). In Fig. 18 (a), cracks are straight slits of about 5–12 μm long and mainly exist in the eutectics structures.

By comparing Fig. 18 (b), it is clearly visible that cracks in Nb modified sample are much less than that of the original sample and microcracks mainly exist in the eutectics.

Ni60 alloy is used in the application where both high hardness and wear resistance are required, therefore it is essential to keep the hardness while tackling the cracking problem. Fig. 19 shows the microhardness of samples with different Nb content. The microhardness was tested on the cross section of the sample. 10 points were randomly tested for each sample. Statistical analysis result is shown in Table 4.

Microhardness of samples with low content of Nb doesn't change significantly. The sample with 2 wt % Nb addition possesses the lowest hardness which is about 702 HV. As shown in Fig. 19, with the addition of Nb, the fluctuation of hardness decreases indicating the improvement of homogeneity.

As mentioned above, the addition of Nb nanoparticles decreases the cracking susceptibility of Ni60 alloy. In order to quantitatively characterize the cracking susceptibility which is related to toughness of the samples, tensile tests were carried out. Fig. 20 (a) shows the stress-strain curves of representative samples in this study. Three samples were tested for each content and the average stress and strain are shown in Fig. 20 (b). It is obvious that the fracture mode of Nb modified samples is brittle fracture, the same as that of original alloy. With the increase of Nb content, the toughness of Ni60 alloy increased slightly.

Fig. 21 shows the SEM images of fractures in Nb modified sample. With the contrast between BSE and SE images in the same area, cleavage fracture of hard phases, quasi-cleavage fracture of eutectics and ductile fracture of Ni can be observed.

4. Discussion

The cracking problem is an important reason to restrict the application of Ni–Cr–B–Si alloy in LMD. To investigate the new method to

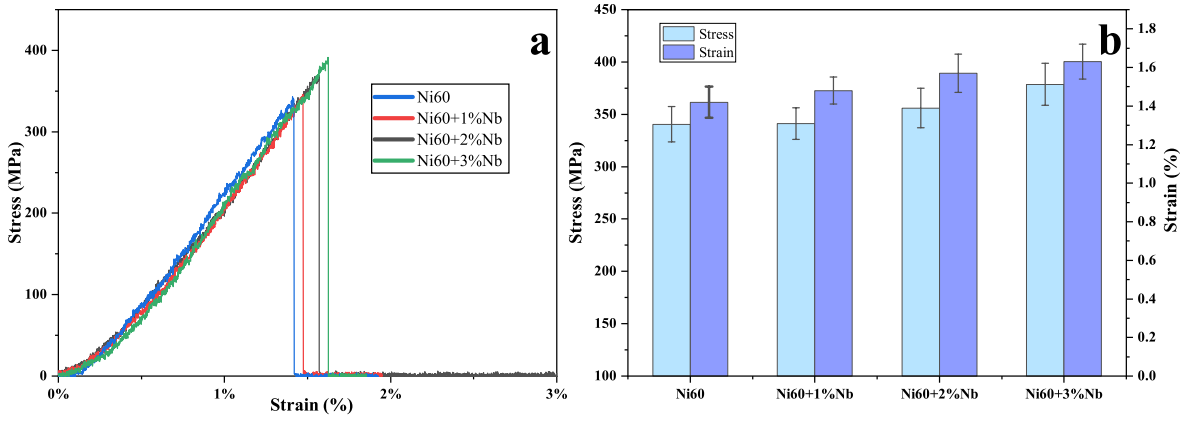

Fig. 20. Stress-strain curves of (a) Ni60 with different Nb addition and (b) the average of strain and stress.

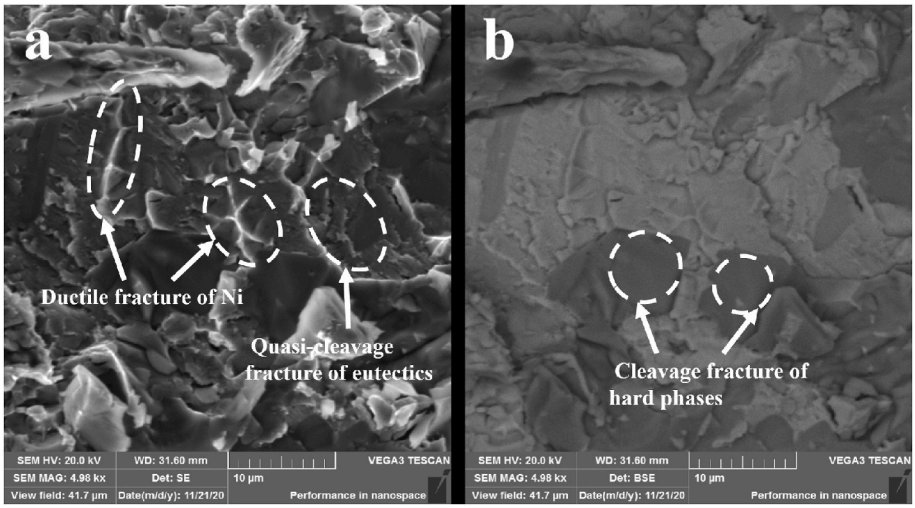

Fig. 21. SEM - (a) BSE and (b) SE images of Ni60 sample with 2 wt % Nb in the same area.

Table 5
Phase formation temperatures according to equilibrium phase diagrams (°C).

Phase	NbC	CrB	Cr_5B_3	Cr_7C_3	$Cr_{23}C_6$	Ni	Ni_3Si	Ni_3B	Ni_3Fe
Temperature °C	3600	2100	1900	1766	1576	1455	1170	1156	517

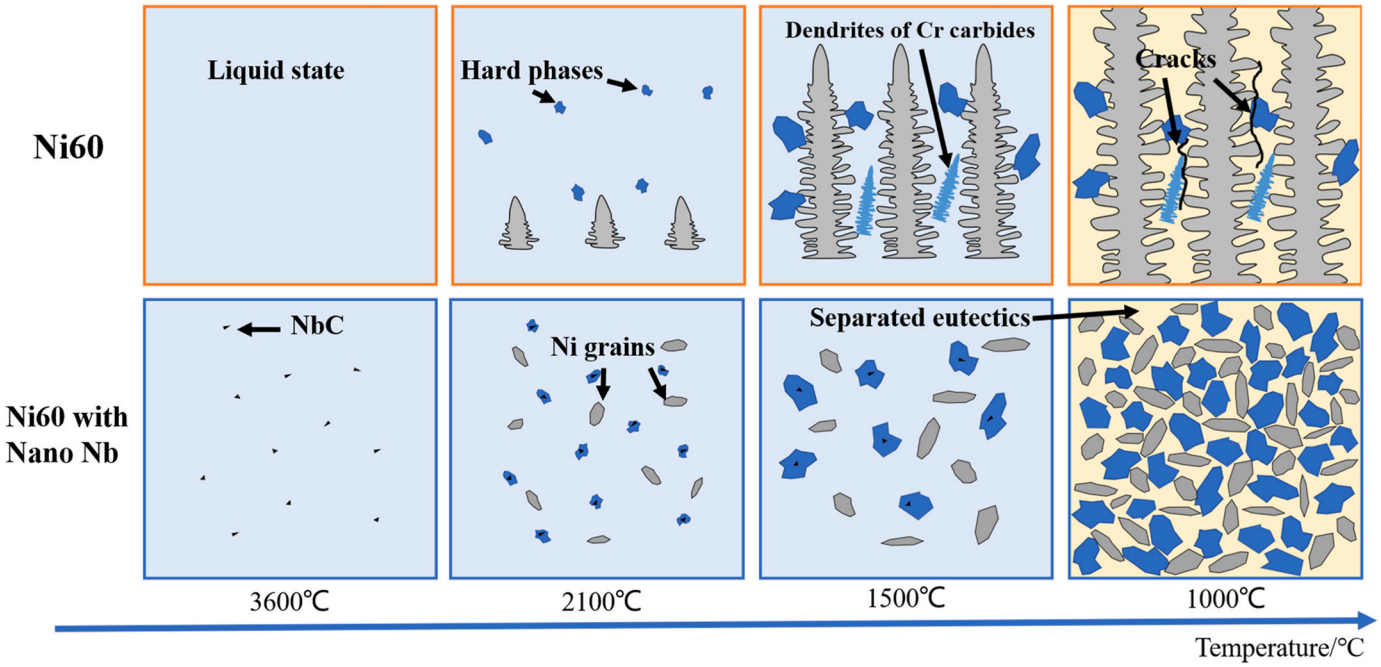

Fig. 22. Schematic representation of solidification of Ni60 alloy and Ni60 modified by Nb nanoparticles.

modify microstructures, Nb nanoparticles were added in Ni60 alloy. It was observed that the addition of Nb nanoparticles modified microstructures of Ni60 alloy and produced NbC nucleation sites thus reducing the cracking susceptibility with little hardness loss. What's more, the addition of Nb nanoparticles was beneficial to reduce the sensitivity of Ni60 alloy to structural fluctuations during remelting hence mostly eliminated layer bands in LMD samples.

Previous researches have reported the microstructure refinement of Cr hard phases (with Nb, Zr or V addition) in Ni–Cr–B–Si alloy, but the cracking tendency did not decrease [23,24]. Addition of Nb, Zr or V produces finer precipitates which should normally result in a decrease of cracking susceptibility according to Griffith theory [22]. A possible explanation for this can be the important contribution of the Ni–B–Si eutectics to cracking susceptibility on laser manufactured Ni–Cr–B–Si alloy.

The eutectics in Ni60 alloy (ratio of Si/B is about 1.25) mostly contain Ni–Ni_3B which is very hard and brittle. Fig. 18 (a) clearly shows the microcracks among the continuous eutectics in LMD Ni60 sample. Based on the findings of this study, the observed reduction of cracking susceptibility in Nb nanoparticles modified samples can be attributed to refinement of columnar dendrites which resulted in a separated eutectic structure as shown in Fig. 15 (b). Table 5 shows the formation temperature of phases in the samples according to equilibrium phase diagrams [27].

During the solidification of Ni60 sample, Cr hard phases formed at first and then Ni dendrites formed. Finally, Ni–B–Si eutectics fill the space between the hard phases and Ni dendrites. Although the solidification rate is relatively high during LMD, it is not sufficient to induce equiaxed growth for a columnar-to-equiaxed transition. As shown in Fig. 22, the growth of columnar dendrites leaves a thin layer of liquid between dendrites leading to cavities. With the cooling of the sample, cracks can initiate from these cavities and grow along the continuous eutectics due to thermal shrinkage.

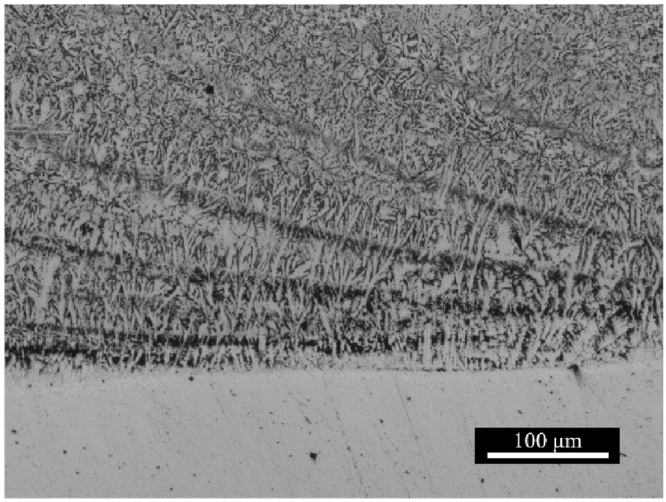

Fig. 23. Dendrites at the bottom of LMD Ni60 sample.

At the bottom of the sample, the cooling condition is very good, so there are a lot of dendrites which grow along the building direction (Fig. 23). Because of the different dilatation coefficient between Ni60 and the substrate, the stress at the junction is very high. This can explain the crack initiation and growth in Fig. 17 (a).

In contrast, samples with Nb nanoparticles addition show equiaxed grains and separated eutectics. Upon melting, Nb nanoparticles were pulled in to the melt pool and NbC were formed in-situ. NbC has a higher

formation temperature in comparison to Cr precipitates and Nb has a higher affinity for B or C than Cr does, providing an ideal heterogeneous nucleation site [19].

As shown in Fig. 22, the large number of nucleation sites induce equiaxed growth of Cr carbides and Ni grains at the same processing parameters of the original alloy. Fine equiaxed Ni grains and Cr hard phases make it easier for grains to rotate in semi-solid structures leading to less strain in the semisolid state. Further, fine equiaxed Ni grains and Cr hard phases separate the continuous eutectics thus prevent the growth of cracks and improve the homogeneity of Ni60 alloy.

It's worth noting that the decrease of crack susceptibility did not induce a significant hardness loss. With the addition of Nb nanoparticles, the hardness of Ni60 alloy slightly decreases. This is a combined influence of Ni grains increasing, continuous eutectics decreasing and Cr hard phases refining. The increase of Ni grains and decrease of continuous eutectics should have deteriorated the hardness, however the refined and uniformly distributed hard phases increase the hardness. As a result, the hardness of Nb nanoparticles modified Ni60 alloy decreases slightly.

As for the reason of improvement in tensile strength, besides the crack susceptibility improvement, the other reason is the morphology changes of hard phases. Cr hard phases change from blocky shape to cluster shape with addition of Nb nanoparticles. Because the cluster-shape hard phases have a better connection with surroundings than blocky phases, combined with the modification of dendrites, tensile stress improved with the addition of Nb nanoparticles as shown in Fig. 20.

For Ni60 alloy, the addition of Nb nanoparticles shows a good effect on tackling the cracking problem. The new method of refining the dendrites and eutectics is an effective way to restrain the cracks. In this study, samples of small size can be built without cracks. To improve the application of the alloy on large size repairing and additive manufacturing, further development can focus on the improvement of alloy composition and the post-treatment technology.

5. Conclusion

We have used Nb nanoparticles in LMD to induce structural refinement of Ni60 alloy which has a very high cracking susceptibility during laser manufacturing, producing crack-free materials with very little hardness loss. The addition of Nb nanoparticles not only refined the hard phases in Ni60 alloy but also converted the columnar dendrites to equiaxed grains leading to a separated eutectic structure, constraining the initiation and growth of cracks. Our approach provides an effective method to tackle the cracking problem of Ni60 alloy and a new mechanism to modified the microstructures of Ni–Cr–B–Si alloy, accelerating the adoption of Ni–Cr–B–Si alloys on additive manufacturing applications.

Funding

This work was supported by the Science and Technology Department of Jilin Province, China (grant number 20200401034GX, 2020C029-1 and SXGJQY2017-14).

Data availability

The data presented in this study are available on request from the corresponding author.

CRediT authorship contribution statement

Liang Liu: Methodology, Writing – original draft, Investigation. **Wenquan Wang:** Conceptualization, Supervision, Funding acquisition. **Xinge Zhang:** Validation, Writing – review & editing. **Xin Li:** Resources. **Yingtao Tian:** Resources. **Xiaohui Zhao:** Resources.

Declaration of competing interest

The authors declare that they have no known competing financial interests or personal relationships that could have appeared to influence the work reported in this paper.

Acknowledgments

Thank Suyu Wang, Yuxin Xu, Ming Du and Yingchao Bi for the writing assistance during the research.

References

[1] I. Hemmati, V. Ocelík, J.T.M. De Hosson, Effects of the alloy composition on phase constitution and properties of laser deposited Ni-Cr-B-Si coatings, Phys. Procedia 41 (2013) 302–311.
[2] N. Serres, F. Hlawka, S. Costil, C. Langlade, F. Machi, An investigation of the mechanical properties and wear resistance of NiCrBSi coatings carried out by in situ laser remelting, Wear 270 (9–10) (2011) 640–649.
[3] C. Wang, Y. Gao, R. Wang, D. Wei, M. Cai, Y. Fu, Microstructure of laser-clad Ni60 cladding layers added with different amounts of rare-earth oxides on 6063 Al alloys, J. Alloys Compd. 740 (2018) 1099–1107.
[4] Z. Chang, W. Wang, Y. Ge, J. Zhou, Z. Cui, Microstructure and mechanical properties of Ni-Cr-Si-B-Fe composite coating fabricated through laser additive manufacturing, J. Alloys Compd. 747 (2018) 401–407.
[5] R. Li, Y. Jin, Z. Li, Y. Zhu, M. Wu, Effect of the remelting scanning speed on the amorphous forming ability of Ni-based alloy using laser cladding plus a laser remelting process, Surf. Coating. Technol. 259 (2014) 725–731.
[6] R. Kaul, P. Ganesh, S.K. Albert, A. Jaiswal, N.P. Lalla, A. Gupta, C.P. Paul, A. K. Nath, Laser cladding of austenitic stainless steel with hardfacing alloy nickel base, Surf. Eng. 19 (4) (2013) 269–273.
[7] I. Hemmati, V. Ocelík, J.T.M. De Hosson, Advances in laser surface engineering: tackling the cracking problem in laser-deposited Ni-Cr-B-Si-C alloys, JOM (J. Occup. Med.) 65 (6) (2013) 741–748.
[8] C.R. Das, S.K. Albert, A.K. Bhaduri, C. Sudha, A.L.E. Terrance, Characterisation of nickel based hardfacing deposits on austenitic stainless steel, Surf. Eng. 21 (4) (2013) 290–296.
[9] D.-s. Wang, E.-j. Liang, M.-j. Chao, B. Yuan, Investigation on the microstructure and cracking susceptibility of laser-clad V2O5/NiCrBSiC alloy coatings, Surf. Coating. Technol. 202 (8) (2008) 1371–1378.
[10] A. Angelastro, S.L. Campanelli, G. Casalino, A.D. Ludovico, S. Ferrara, A methodology for optimization of the direct laser metal deposition process, Key Eng. Mater. 473 (2011) 75–82.
[11] A. Angelastro, S.L. Campanelli, A.D. Ludovico, Characterization of colmonoy 227-F samples obtained by direct laser metal deposition, Adv. Mater. Res. 83–86 (2009) 842–849.
[12] C.P. Paul, A. Jain, P. Ganesh, J. Negi, A.K. Nath, Laser rapid manufacturing of Colmonoy-6 components, Opt Laser. Eng. 44 (10) (2006) 1096–1109.
[13] K. Osakada, M. Shiomi, Flexible manufacturing of metallic products by selective laser melting of powder, Int. J. Mach. Tool Manufact. 46 (11) (2006) 1188–1193.
[14] W. Wang, L. Liu, X. Zhang, Z. Shi, Y. Tian, J. Lin, Microstructures and mechanical properties of Ni60 alloy fabricated by laser metal deposition, Mater. Res. Express 7 (1) (2020).
[15] N. Ahmed, Direct metal fabrication in rapid prototyping: a review, J. Manuf. Process. 42 (2019) 167–191.
[16] T.D. Ngo, A. Kashani, G. Imbalzano, K.T.Q. Nguyen, D. Hui, Additive manufacturing (3D printing): a review of materials, methods, applications and challenges, Compos. B Eng. 143 (2018) 172–196.
[17] C. Sudha, P. Shankar, R.V.S. Rao, R. Thirumurugesan, M. Vijayalakshmi, B. Raj, Microchemical and microstructural studies in a PTA weld overlay of Ni–Cr–Si–B alloy on AISI 304L stainless steel, Surf. Coating. Technol. 202 (10) (2008) 2103–2112.
[18] I. Hemmati, V. Ocelík, J.T.M. De Hosson, Toughening mechanism for Ni–Cr–B–Si–C laser deposited coatings, Mater. Sci. Eng., A 582 (2013) 305–315.
[19] I. Hemmati, R.M. Huizenga, V. Ocelík, J.T.M. De Hosson, Microstructural design of hardfacing Ni–Cr–B–Si–C alloys, Acta Mater. 61 (16) (2013) 6061–6070.

[20] I. Hemmati, V. Ocelík, K. Csach, J.T.M. De Hosson, Microstructure and Phase formation in a rapidly solidified laser-deposited Ni-Cr-B-Si-C hardfacing alloy, Metall. Mater. Trans. 45 (2) (2013) 878–892.
[21] I. Hemmati, J.C. Rao, V. Ocelík, J.T.M. De Hosson, Phase formation and properties of vanadium-modified Ni–Cr–B-Si–C laser-deposited coatings, J. Mater. Sci. 48 (8) (2013) 3315–3326.
[22] R.A. Ibrahim, Fundamentals of Fracture Mechanics, Wiley, 1973.
[23] T. Yu, Q. Deng, G. Dong, J. Yang, Effects of Ta on microstructure and microhardness of Ni based laser clad coating, Appl. Surf. Sci. 257 (11) (2011) 5098–5103.
[24] M.-J. Chao, E.-J. Liang, Effect of TiO2-doping on the microstructure and the wear properties of laser-clad nickel-based coatings, Surf. Coating. Technol. 179 (2–3) (2004) 265–271.
[25] J.H. Martin, B.D. Yahata, J.M. Hundley, J.A. Mayer, T.A. Schaedler, T.M. Pollock, 3D printing of high-strength aluminium alloys, Nature 549 (7672) (2017) 365–369.
[26] A. Angelastro, S.L. Campanelli, G. Casalino, Statistical analysis and optimization of direct metal laser deposition of 227-F Colmonoy nickel alloy, Opt Laser. Technol. 94 (2017) 138–145.
[27] J.L. Murray, ASM handbook: alloy phase diagrams, Am. Soc. Microbiol. News 3 (1992) 226–290.